Journal of Molecular Liquids 394 (2024) 123721

Contents lists available at ScienceDirect

Journal of Molecular Liquids

journal homepage: www.elsevier.com/locate/molliq

Hydrogel based on patch halloysite nanotubes: A rheological investigation

Martina Maria Calvino [a], Giuseppe Cavallaro [a,*], Pooria Pasbakhsh [b], Giuseppe Lazzara [a], Stefana Milioto [a]

[a] Dipartimento di Fisica e Chimica, Università degli Studi di Palermo, Viale delle Scienze, pad. 17, 90128 Palermo, Italy
[b] Department of Mechanical Engineering, School of Engineering, Monash University Sunway Campus, Bandar Sunway 47500, Selangor, Malaysia

ARTICLE INFO

Keywords:
Halloysite nanotubes
Rheology
Hydrogel
Patch halloysite

ABSTRACT

The rheological behaviour of Patch halloysite nanotubes (PT_Hal) was investigated here. Their peculiar morphology shows longer and thinner nanotubes and gives rise to the formation of gel-like systems that are not evidenced in halloysite from other natural sources. According to frequency sweep tests, PT_Hal possesses solid-like characteristics even at low concentrations, suggesting that the material is highly structured. Interestingly, flow ramp analysis evidenced two distinct behaviours based on the clay concentration: a yield stress was detected only from 0.75 wt%, indicating the sample's ability to resist deformation or breaking. Furthermore, the study investigated the influence of ionic strength, revealing that the addition of salt did not significantly affect the gel's properties of this clay. Accordingly, in this work we propose a new hydrogel system based on green nanoclays that can be suitable for industrial and biological applications as well as for cultural heritage.

1. Introduction

Halloysite is a naturally occurring nanoclay with a unique hollow tubular structure. Generally, the length of halloysite nanotubes is approximately 1 μm, while the external and internal diameters vary within the ranges of 20 to 200 nm and 10 to 70 nm, respectively. Its properties and characteristics, such as the sizes, specific surface and polydispersity are influenced by the geological deposit from which they are sourced [1]. Among them, the Patch halloysite (PT_Hal), sourced from Western Australia, is acknowledged as a highly pure variety of halloysite (content of ca. 96 %) [2]. These nanotubes exhibit thinner tubes and an exceptional length extending up to 30 μm. Moreover, they also stand up for their fibrous structure forming clusters that appear as patches. It is worth noting that the external and internal surfaces of halloysite have distinct chemical properties, with the former being negatively charged and the latter being positively charged across a wide pH range [3].

This characteristic enables the loading of negative molecules into the inner lumen and the interaction of positive active species with the outer surface. Halloysite also represents a versatile nanofiller that can be incorporated into biopolymeric matrices [4–6], obtaining green nanocomposite materials suitable for a wide range of applications, including medicine [7–10], cosmetics [11,12], packaging [13–15] and environmental remediation [16–25]. Moreover, halloysite nanotubes are effective as catalytic supports [26–32], additives for metal batteries [33,34] and nanocarriers for functional molecules with biological and chemical activities [35–39].

Most research studies exploring the use of halloysite nanotubes as nanomaterials have focused on halloysite derived from one of the primary sources, typically New Zealand or USA, but its properties can differ based on its origin, owing to the distinct local conditions under which it was formed [40]. For instance, Makaremi et al. [40] demonstrated that shorter nanotubes showed superior capacity in encapsulating salicylic acid within their hollow structure compared to patchy and longer halloysite nanotubes as they require additional time and energy to have the active molecule loaded in the tubes. On the other hand, it is known that halloysite does not form gel itself. Actually, Luo et al. [41] proved that the sol–gel transition occurs at a concentration of ca. 40 wt% and the aqueous dispersion exhibits a pH-induced gelation when hydrochloric acid is added, due to the reduced repulsive electrostatic forces between the nanotubes.

Thus, our study wants to point out that, thanks to its peculiar fibrous structure, Patch has different rheological features with respect to halloysite from other natural sources. Accordingly, a rheological study on patch halloysite samples at different concentrations is presented here.

In addition, literature reports that the colloidal stability of nanoclays can be influenced by several factors, including the addition of polymers [42,43] as well as the ionic strength [44]. Moreover, changing the ionic

* Corresponding author.
E-mail address: giuseppe.cavallaro@unipa.it (G. Cavallaro).

https://doi.org/10.1016/j.molliq.2023.123721
Received 16 October 2023; Received in revised form 24 November 2023; Accepted 30 November 2023
Available online 4 December 2023

strength in a system can also have significant effects on gel-like structures [45,46], such as swelling [47], increased stability [48] or viscosity due to stronger interactions with the components of the gel [49]. Since, according to the literature, NaCl concentration affects the settling velocity of halloysite dispersions, we also investigated its influence in the PT_Hal hydrogels in this study.

2. Materials and methods

2.1. Materials

Ultra HalloPure Halloysite (UP_Hal) was a gift by I-Minerals Inc. mined in the geological deposit of Latah County.

(NW Idaho, North America) and Patch Halloysite (PT_Hal) (Kalgoorie, Western Australia) is a kind donation provided by Dr. Keith Norrish from his collection and research on Patch (CSIRO Soils, Adelaide). NaCl (>99 %, CAS 7647–14-5) and NaOH pellets (≥98 %, CAS 1310–73-2) were Sigma Aldrich products.

2.2. Patch halloysite purification

The separation of coarse impurities was performed by following a procedure reported elsewhere for PT_Hal samples [1,2]. In particular, 5 g of PT_Hal were grounded in a mortar. The obtained powder was dispersed in deionized water and the pH was set between 7.5 and 8 by using a sodium hydroxide solution 0.1 M. Several cycles of sonication and washing in 1.5 L of water were carried out to purify the sample. After that, the dispersion was filtered by a peristaltic pump to exclude coarse residuals and dried at 50 °C for 48 h.

2.3. Hydrogel preparation

Patch halloysite, after purification, was dispersed in deionized water at different concentrations: 0.005, 0.1, 0.5, 0.75, 1 and 2 wt%. Then, samples were sonicated for 15 min and stirred for 48 h to avoid the formation of aggregates.

The same procedure was performed to prepare UP_Hal samples for comparison at 1 wt%.

Patch halloysite nanotubes were added to NaCl aqueous solutions at four different concentrations (10^{-1}, 10^{-2}, 10^{-3} and 10^{-4} M) and the obtained dispersions were sonicated for 15 min and magnetically stirred for 2 days.

2.4. Methods

2.4.1. Thermogravimetric analysis (TGA)

Thermogravimetric experiments were carried out using a Q5000 IR apparatus (TA Instruments) under inert atmosphere using nitrogen flows of 25 and 10 cm^3 min^{-1} for the sample and the balance, respectively. Samples were heated in a platinum pan from room temperature to 800 °C with a scanning rate of 20 °C min^{-1}.

2.4.2. X-ray Fluorescence (XRF)

X-ray Fluorescence (XRF) Spectrometry was performed using an Olympus Innov X DS-2000 Delta Standard Alloy XRF Handheld Analyzer operating in the Alloy Plus analysis mode.

2.4.3. ζ-Potential

ζ-Potential measurements were performed by means of a Zetasizer NANO-ZS (Malvern Instruments) under isothermal conditions at 25.0 ± 0.1 °C. The tests were carried out by using a disposable folded capillary cell and the concentration of PT_Hal dispersion was 0.001 wt%. The ζ-potential was calculated using the Smoluchowski approximation, which is considered an accurate approximation for particles larger than 0.2 μm in aqueous solutions. All experiments were replicated three times, and the average values were reported.

2.4.4. X-ray diffraction (XRD)

The patterns were obtained from an X-ray diffractometer (Rigaku, MiniFlex) with a CuKa radiation source including a nickel filter and working at 40 kV and 15 mA. The wavelength of the X-ray beam was 1.5406 Å, and the layer spacing of the samples was calculated by the Bragg's equation, which can be expressed as

$$n\lambda = 2d\sin\theta \quad (1)$$

where θ is the angle that the outgoing beam forms with the crystalline layer, λ is the wavelength of the radiation, d is the distance between two adjacent layers and n can be 1,2 or 3.

The angle for scanning ranged from 2° to 70° with a rate of 20° min^{-1} and a step of 0.02°.

2.4.5. Scanning electron microscopy

The ultra-high resolution field emission scanning electron microscope (FE-SEM, Hitachi SU8010) was used to observe the morphologies of halloysite nanotubes. A thin layer of platinum was applied to coat the samples in order to avoid electrostatic charging. Additionally, the morphology of halloysite nanotubes was also observed using the transmission mode (STEM) of the same FE-SEM instrument with a voltage of 30 kv.

2.4.6. Rheology

The rheological characterization of PT_Hal dispersions was studied using a Discovery HR-1 rheometer (TA Instruments) with a parallel plate geometry (800–1000 μm gap and 20 mm diameter). Amplitude sweep, frequency sweep and flow ramp stress tests were performed after conditioning the sample at 25 °C. The amplitude sweep tests were conducted at a constant angular frequency of 100 rad s^{-1} while increasing the oscillation strain from 0,001 % and 100 %. For frequency sweep tests, the angular frequency was ranged from 0.1 to 100 rad s^{-1} at a fixed strain amplitude of 0.1 %. Flow ramp tests were instead performed increasing the stress from 0 to 50 Pa.

3. Results and discussion

3.1. Patch purification

XRF measurement allowed to obtain the chemical composition of UP_Hal and PT_Hal before and after the purification. As reported in Table 1, PT_Hal not purified (PT_Hal_NP) presents lower silicon content than the same sample after purification (PT_Hal_P) which has an enrichment of 6 % in silicon. Moreover, PT_Hal_P shows a decrease of the amount of Ti, Mg, Cr and Mn. On the other hand, iron content is nearly constant after purification, and it is present in a minimal amount.

It has been previously reported [2,50] that patch halloysite samples usually contain less than 1 % of iron. Actually, we found a value of 2.52 % in PT_Hal_NP that can be attributed to the different levels of iron oxide contamination. As a matter of fact, Churchman et al. [50] stated that, even if iron is not part of the structure, it can influence the size of halloysite particles by restraining crystal growth. The substitution of the smaller Al^{3+} ion with the larger Fe^{3+} ion in the octahedral sheet of

Table 1
Chemical composition of UP_Hal and PT_Hal samples before and after the purification.

Sample	Al/wt %	Si/wt %	Mg/ wt%	Fe/wt %	Ti/wt %	Cr/wt %	Mn/ wt%
UP_Hal	41.7 ± 0.4	52.1 ± 0.4	1.4 ± 0.6	3.89 ± 0.09	0.8 ± 0.1	ND	0.08 ± 0.02
PT_Hal_P	41.1 ± 0.3	53.5 ± 0.3	1.2 ± 0.4	2.99 ± 0.06	0.47 ± 0.09	0.18 ± 0.02	ND
PT_Hal_NP	41.05 ± 0.4	46.8 ± 0.4	2.2 ± 0.6	2.52 ± 0.07	6.7 ± 0.2	0.20 ± 0.03	0.07 ± 0.01

halloysite can also happen with high levels of Fe_2O_3 (ca. 4 %) leading to more planar layers as in kaolinite. This is reflected by the fact that halloysite with long tubular particles tends to contain low Fe content whereas shorter and approximately platy particles often contain high levels of structural Fe, as demonstrated by the results reported in Table 1 for UP_Hal. Moreover, besides the amount of iron, it showed very similar chemical composition compared to PT_Hal. In general, the obtained XRF results are also in agreement with literature data reported elsewhere [51] for halloysite nanotube samples.

Thermogravimetric curves of UP_Hal, purified and not purified PT_Hal are reported in Fig. 1. All the samples exhibited the two mass losses typical of halloysite: the first one until 150 °C and the second one in the range between 350 and 550 °C, respectively related to physically adsorbed water molecules and the dehydroxylation of aluminium inner sheets. The residual mass at 800 °C and the mass losses at each step (30–150 °C and 350–550 °C) are reported in Supporting Information (Table S1). Concerning the first mass loss, UP_Hal showed the lowest value (1.17 %) compared to the PT_Hal samples. Furthermore, the main difference between the two samples of Patch halloysite is related to the percentage of the first mass loss and consequently the residual mass at 800 °C. It is equal to 82 % for the purified PT_Hal and 79 % for the not purified PT_Hal. During the purification protocol, impurities have been washed away and consequently, we observed a lower value of residual mass in PT_Hal_P. On the other hand, the second mass loss is comparable for the three investigated samples.

3.2. Comparison between PT_Hal and UP_Hal

Before deeply analysing the rheological behavior of these peculiar clays, we focused our attention on the differences occurring between them.

A morphological characterization of PT_Hal and UP_Hal is presented in Fig. 2. SEM micrographs reveal that PT_Hal exhibits much greater length and thinness of the tubes. They are characterized by outer diameters ranging from 40 to 55 nm, inner diameters between 12 and 22 nm and lengths ranging from 200 to 30,000 nm. Moreover, PT_Hal tubes are entangled and bent, forming a structure similar to a bird nest. Since the walls are very thin, they are susceptible to breakage into shorter fragments, but still intact tubes can be observed as bundles of tightly packed parallel tubes.

On the other hand, UP_Hal, possesses shorter and stubby tubes ranging in length from 100 nm to 2 μm, while the outer diameter ranges between 100 and 200 nm and the inner diameter between 10 and 70 nm (Fig. 2.(g)).

X-ray diffraction patterns of both UP_Hal and PT_Hal exhibited the typical diffraction pattern of dehydrated halloysite (Fig. S1). The dehydration of Patch was previously reported [52] by following the continuous collection of XRD patterns whilst in situ heating and it was showed that the dehydration produces some irregular d-spacings probably due to the interstratification of hydrated and dehydrated halloysite layers and the interference between the regular flattened tubes with ca. 8 Å d-spacing. In particular, peaks were observed at 2θ = 12.0, 19.9, 24.7, 35.0, 38.3, 54.9 and 62.4 corresponded to (001), (100), (002), (110), (003), (210) and (300) planes, respectively [53]. The (001) plane corresponds to a basal spacing of 0.72 nm, which identifies these samples as halloysite-(7 Å).

Traces of quartz were identified only in the PT_Hal sample, corresponding to a sharp peak at 2θ = 26° and 60°.

A qualitative evaluation of the gel formation is shown in Fig. 3. We reported the images of PT_Hal and UP_Hal 1 wt% before and after the inversion. Despite the same concentration of PT_Hal, it is stable to the tube inversion test showing a gel-like structure compared to the same or even higher concentrations of UP_Hal in which it is not evidenced.

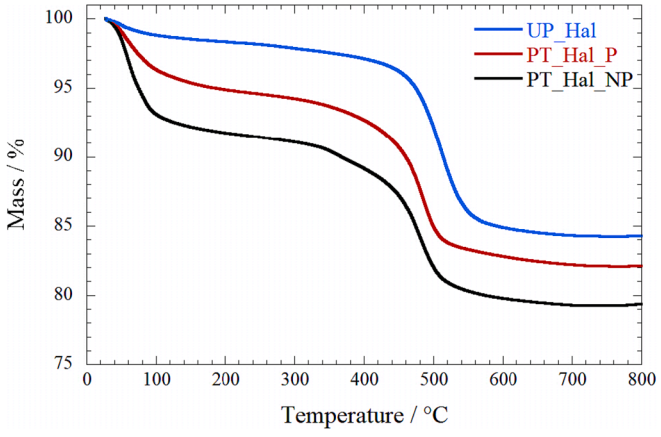

Fig. 1. Thermogravimetric curves of UP_Hal, non-purified (PT_Hal_NP) and purified (PT_Hal_P) Patch Halloysite.

3.3. Rheological characterization of PT_Hal

Aimed to characterize the viscoelastic behavior of the clay, amplitude sweep tests were performed by measuring the strain amplitude dependence of the storage and loss moduli (G', G").

In Fig. 4 we reported two concentrations as examples of the more comprehensive concentration range investigated in this work, just to show the linear viscoelastic regions. Namely, below 10 % strain, G' is higher than G", for both PT_Hal at 1 and 2 wt%, suggesting a gel-like structure. As a matter of fact, in this region both moduli remain constant, indicating the presence of the linear viscoelastic region. The crossover strain points are clearly displayed after 10 % strain and their values were calculated determining the point at which G'=G". As shown in Fig. 4, the crossing points between G' and G" moduli are shifted to higher oscillation strain by increasing the clay concentration. Specifically, they are at 16.30 % and 45.52 % for PT_Hal 1 and 2 wt%, respectively.

Having pinpointed the linear viscoelastic regions, angular frequency sweep tests were performed, imposing a constant strain on the systems at variable frequency. Usually, frequency sweep curves give a rheological description of the product behavior during storage and application [54–56]. The obtained rheological data are displayed in Fig. 5a), showing G' and G" moduli as a function of the angular frequency. As a general result, the storage modulus (G') is larger than the loss modulus (G") in the entire range of frequency. Namely, for a gel-like material G' and G" curves are constant, remarking that PT_Hal behaves like a solid and suggesting that the material is highly structured starting from a concentration of 0.75 wt%. High frequencies correspond to short time scales and low frequencies to longer time scales. This means that the gel-like structure is time-independent [57,58], highlighting their stability over time. Moreover, Fig. 5b) shows that increasing the concentration both moduli increase and the G' medium values are higher than G" from 0.005 wt% along the angular frequency range investigated.

We calculated the average tanδ values within the angular frequency range between 0.1 and 100 rad s^{-1} by G''/G' ratios. The obtained data (see Supporting Information) confirmed the solid-like behavior of the hydrogels being that tanδ is lower than 0.1 for all the investigated dispersions. We detected that tanδ is nearly constant throughout the entire concentration range highlighting the predominance of the elastic contribution.

The viscosity as a function of the shear rate can provide relevant information about its performance and processing. With this in mind, flow curves are reported in Fig. 6. The viscosity displays higher values increasing the concentration of the clay. Accordingly, the most considerable difference is evidenced for PT_Hal 2 wt%, which presents an order of magnitude of increment with respect to 1 wt%. It is clear that the microstructure plays a crucial role in determining the rheological behavior of the system. In this case, two phenomena should be taken

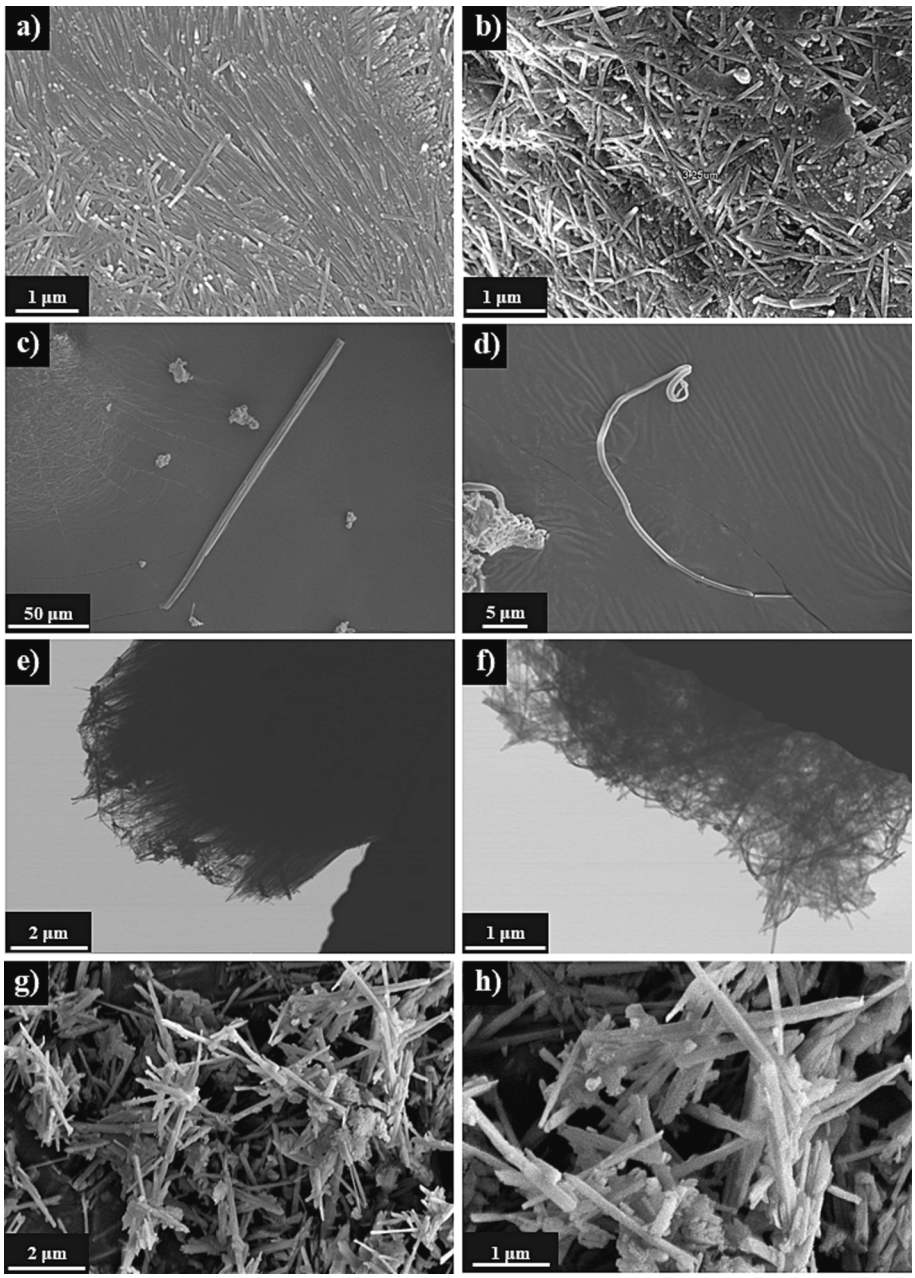

Fig.2. Morphological properties of pure Patch and UltraPure Halloysite. (a-d) Scanning electron microscopy micrographs of PT_Hal_P (e-f) Scanning transmission electron microscopy micrographs showing patchy entangled halloysite nanotubes of PT_Hal_P (g) Scanning transmission electron microscopy micrographs of UP_Hal.

Fig. 3. Inversion test of PT_Hal and UP_Hal 1 wt%.

into consideration to explain the rheology of Patch halloysite.

The first is that increasing the concentration, the interactions between the nanotubes are enhanced promoting a higher viscosity of the system. Another crucial factor is represented also by the presence of a bird nest structure in PT_Hal in which the nanotubes are entangled with each other and bent[40], reducing the free water diffusion between the nanotubes. In this regard, geometrical considerations can give a more comprehensive view about the influence of the tube's morphology on the rheology. We can consider a contact distance given by the average length of the nanotubes and assume a simple cubic model to calculate the critical overlapping volume fraction φ*:

$$\varphi^{*} = \pi R^2 / L^2 \tag{2}$$

where R and L are the external radius and the length of the nanotubes, respectively. Volume fraction values of ca. 4–10 % for aqueous dispersions of halloysite from Dragon Mine have been previously reported [3].

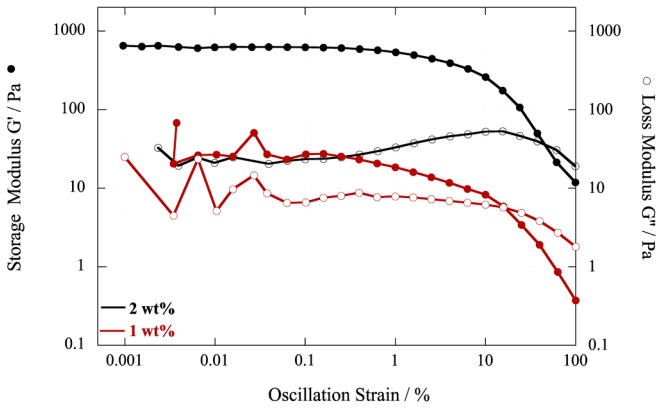

Fig. 4. Amplitude sweep tests of PT_Hal. Full and empty symbols indicate Storage modulus (G') and Loss modulus (G"), respectively.

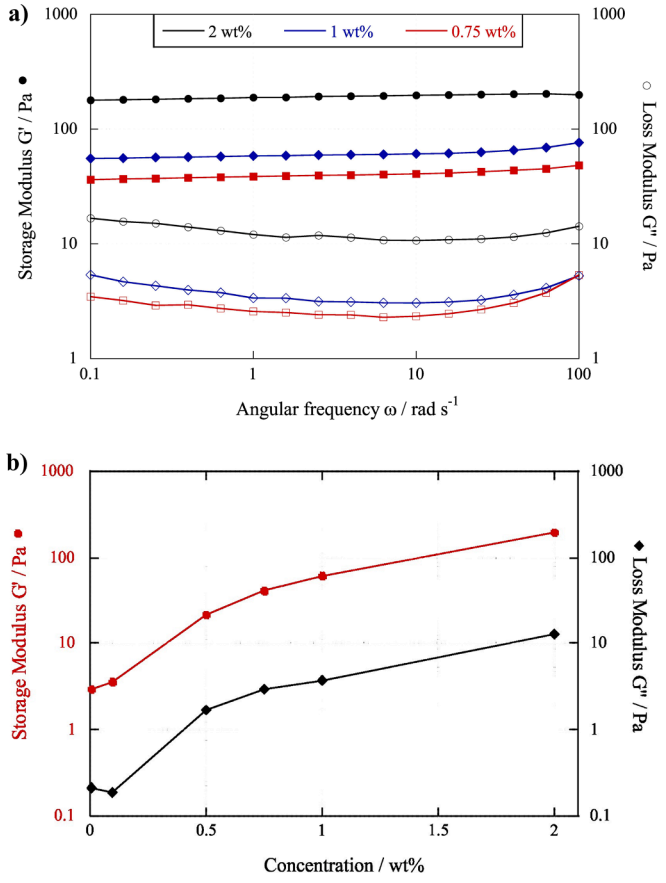

Fig. 5. A) results of angular frequency sweep tests on pt_hal at 2, 1 and 0.75 wt %. Full and empty symbols indicate Storage modulus (G') and Loss modulus (G"), respectively. b) Storage and Loss moduli as a function of the clay concentration.

Here, the calculated φ*, by considering average values for R and L [2], are 3.1 % for UP_Hal and 0.03 % for PT_Hal. This means that the volume required to generate the nanotubes entanglement is 100 times lower for PT_Hal than UP_Hal. Namely, the critical concentration for the hydrogel formation is reached at lower concentration for PT_Hal samples with respect to shorter and stubby halloysite clay nanotubes.

Moreover, the presence of this network-like structures in PT_Hal, reduces the fluid flow, contributing to the higher viscosity of the system [59,60].

On the other hand, the viscosity below 0.75 wt% assumes low values

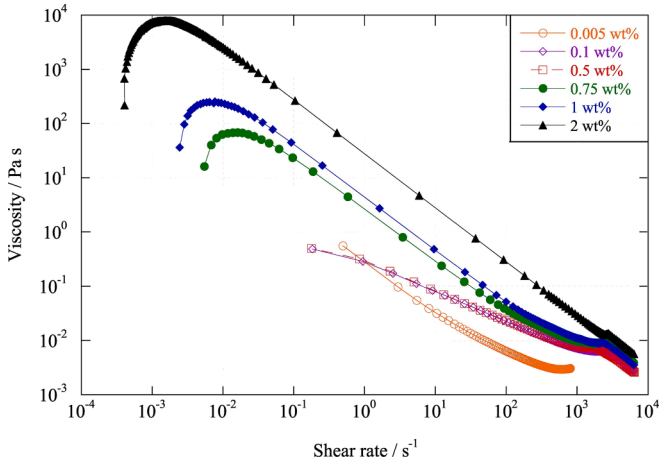

Fig. 6. Flow ramp tests showing the viscosity as a function of the shear rate.

pointing out that the network is not structured as in 1 wt%. As a result of this transition, the material undergoes a change from an apparently solid state to a liquid state, allowing it to flow easily. All the samples, starting from a shear stress of 0.1 s^{-1} exhibited shear thinning, as represented by the decrease of viscosity with increasing the shear rate. This phenomenon is requested in hydrogel for biomedical applications since they should exhibit viscous flow under shear stress and self-healing properties as reported elsewhere [61,62].

It should be noted that PT_Hal 0.75, 1 and 2 wt% at very low shear rate exhibited an increase of the viscosity up to a critical value, beyond which it decreases. Thus, this indicates the presence of yield stress that is better evidenced in Fig. 7, where the shear stress as a function of the shear rate is reported.

Accordingly, the yield stress reflects the resistance of the sample structure to deformation or break and it is detected starting from PT_Hal 0.75 wt%. The flow begins when an applied stress is strong enough to disturb the gel-like structure of the material, resulting in a significant decrease in viscosity, as previously shown in Fig. 6. This is better highlighted by looking at the inset in Fig. 7, where the yield stress is not evidenced up to a concentration of 0.5 wt% and these curves start from 0 Pa, meaning that the material flows and it is easily deformable. On the contrary, the yield stress of PT_Hal 2 wt% is remarkable as it is significantly higher than less concentrated samples, reaching a value of ca. 28 Pa (Table 2).

Thus, we can state that PT_Hal is a non-Newtonian fluid and specifically, it can be classified as a Pseudoplastic fluid at low concentration and as Bingham Plastic fluid at concentrations greater than 0.5 wt%.

To better investigate the rheological properties of Patch halloysite, the Carreau (Eq. (3)) and Carreau-Yasuda models (Eq. (4)) were applied to the experimental flow curves obtaining the fitting parameters reported in Table S3.

$$\frac{\eta-\eta_\infty}{\eta_0-\eta_\infty}=\frac{1}{\left[1+(k\dot{\gamma})^2\right]^{\frac{n}{2}}} \tag{3}$$

$$\frac{\eta-\eta_\infty}{\eta_0-\eta_\infty}=\left[1+(k\dot{\gamma})^a\right]^{\frac{n-1}{a}} \tag{4}$$

Here, η_0 is the viscosity at zero shear rate, η_∞ is the viscosity at infinite shear rate, k represents the consistency index or relaxation time and n and a are two dimensionless parameters. The Carreau-Yasuda model is an extension of the Carreau model. In particular, the main difference between the two models is linked to the ability to capture shear thinning or thickening behaviours. The Carreau model is usually referred to as shear thinning, meaning that the fluid viscosity decreases as the shear rate increases. In contrast, the Carreau Yasuda model is used for both shear thinning and thickening behaviours [63]. The presence of yield

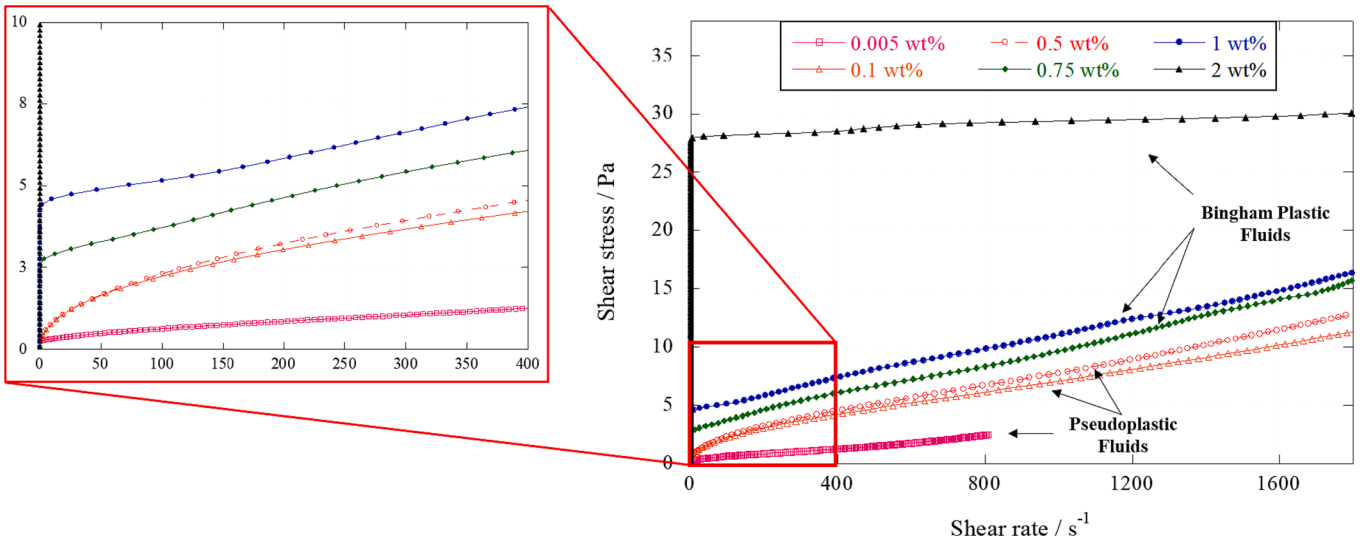

Fig. 7. Shear stress as a function of the shear rate. The inset shows a magnification highlighting different types of flow behaviour.

Table 2
Yield stress values.

Sample	Yield Stress σ_0/Pa
PT_Hal 0.005 wt%	0
PT_Hal 0.1 wt%	0
PT_Hal 0.5 wt%	0
PT_Hal 0.75 wt%	3.07
PT_Hal 1 wt%	4.69
PT_Hal 2 wt%	28.08

stress led to the Carreau Yasuda model to better fit the analysed curves as reported in Supporting Information (Table S3).

An increase in zero-shear rate viscosity and consistency with increasing PT_Hal concentration is detected and showed in Fig. 8.

3.4. Effect of ionic strength

The ionic strength can have a strong impact on gel-like structures, and it was widely reported in literature [64,65]. For example, it has been demonstrated that the addition of NaCl can weaken the gel structure of cellulose nanocrystal suspensions and decrease the viscosity as well [66]. With this in mind, the effect of ionic strength on the investigated gels was evaluated. Accordingly, flow ramp tests performed on PT_Hal 1 wt% in water and at different NaCl concentrations are reported in Fig. 9. It can be noted that the gel-like network is not destroyed by adding the

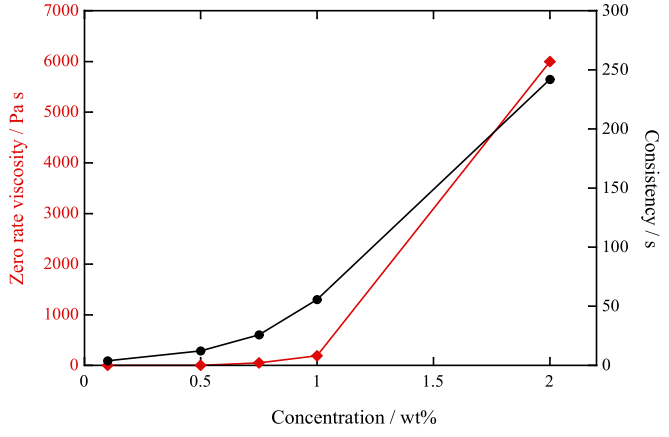

Fig. 8. Zero-shear rate viscosity and consistency as a function of concentration.

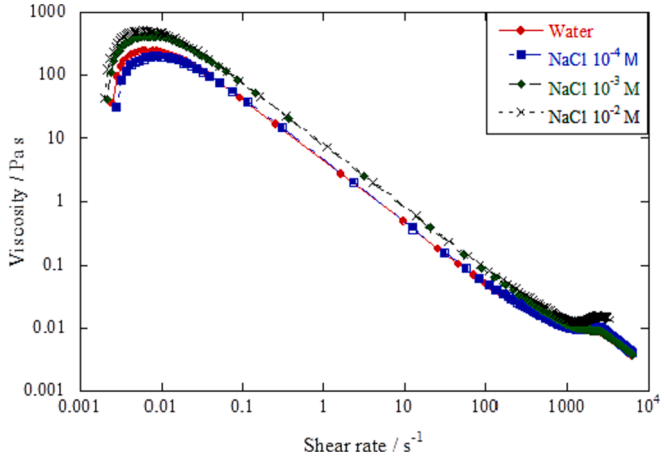

Fig. 9. Flow ramp tests. Viscosity as a function of the shear rate for PT_Hal 1 wt % in water and NaCl at different concentrations.

salt and with respect to water, lower concentrations of NaCl do not affect the rheology properties. As a matter of fact, the viscosity curves of PT_Hal in water and in NaCl 10^{-4} M are overlapped. There is a small effect of ionic strength increasing the NaCl concentration evidenced by a minimal increase of viscosity.

ζ potential measurements were carried out in order to have information about the surface charge of the nanotubes. As reported by Cavallaro et al.[44], although Hal from different natural sources can show similar responses to salt addition, they present differences in the effective charge that can influence their colloidal stability. The surface charge (σ) was estimated from the ζ potential values as established by the Grahame equation:

$$\sigma = (8RT\varepsilon\varepsilon_0 C)^{\frac{1}{2}} \sinh\left(\frac{Ze\zeta}{2k_bT}\right) \quad (5)$$

where ε is the solvent relative dielectric constant, ε_0 is the vacuum dielectric constant, C is the bulk concentration of electrolyte, e is the electron elemental charge, and Z is 1 for NaCl.

As shown in Table 3, the addition of NaCl generated a slight decrease of the absolute value of ζ potential for PT_Hal. These results can be explained by considering the screening effect of Na^+ ions towards the negative surface charge of PT_Hal. Namely, the presence of the

Table 3
ζ Potential PT_Hal samples in water and NaCl.

Sample	ζ Potential/mV	Surface charge σ/mC m^{-2}
PT_Hal	−17.5	/
PT_Hal/NaCl 10^{-4} M	−15.5	$1.13 \cdot 10^{-5}$
PT_Hal/NaCl 10^{-2} M	−14.0	$1.02 \cdot 10^{-4}$

electrolyte in the aqueous medium caused a reduction of the Debye length inducing a decrease of ζ potential absolute value. As expected, the screening effect was enhanced by increasing the ionic strength of the aqueous dispersion. Similar results were observed for halloysite nanotubes from other sources (Matauri Bay and Dragon Mine) [44].

4. Conclusions

This work aims to characterize PT_Hal clay samples from a rheological point of view, highlighting that clay microstructure plays a key role on it. As a matter of facts, their different morphology led to peculiar physico-chemical properties that are not evidenced in UP_Hal. PT_Hal shows thinner and longer tubes creating a structure similar to a bird nest allowing the formation of gel-like structures. It was proved by dynamic viscoelastic tests that PT_Hal is a non-Newtonian fluid and G' is higher than G", meaning that the system is highly structured. Flow curves provided information about the viscosity related to shear rates, which is crucial in the production field where the product is subjected to stirring and pumping processes and namely different shear rates. Accordingly, two different behaviours were evidenced depending on the clay concentration: from 0.75 wt% a yield stress is detected, reflecting the sample's ability to withstand deformation, or breaking. The effect of ionic strength was also evaluated, showing that the addition of salt doesn't affect the properties of the gel since there isn't a significant change in both ζ potential and viscosity of PT_Hal samples.

CRediT authorship contribution statement

Martina Maria Calvino: Investigation, Data curation, Writing – original draft. **Giuseppe Cavallaro:** . **Pooria Pasbakhsh:** Data curation, Writing – original draft. **Giuseppe Lazzara:** Conceptualization, Supervision. **Stefana Milioto:** Funding acquisition, Resources.

Declaration of Competing Interest

The authors declare that they have no known competing financial interests or personal relationships that could have appeared to influence the work reported in this paper.

Data availability

Data will be made available on request.

Acknowledgments

The work was financially supported by FFR 2023 and University of Palermo.

This work was funded by the European Union (NetGeneration EU) through the MUR-PNRR project SAMOTHRACE (ECS00000022).

We also thank John Keeling (EX: Geological Survey of South Australia) and Jock Churchman (University of Adelaide) for the given support to Pooria Pasbakhsh (one of the co-authors of this paper) during his research on halloysite in 2010.

Appendix A. Supplementary material

Supplementary data to this article can be found online at https://doi.org/10.1016/j.molliq.2023.123721.

References

[1] G. Cavallaro, L. Chiappisi, P. Pasbakhsh, M. Gradzielski, G. Lazzara, A structural comparison of halloysite nanotubes of different origin by Small-Angle Neutron Scattering (SANS) and Electric Birefringence, Appl. Clay Sci. 160 (2018) 71–80, https://doi.org/10.1016/j.clay.2017.12.044.
[2] P. Pasbakhsh, G.J. Churchman, J.L. Keeling, Characterisation of properties of various halloysites relevant to their use as nanotubes and microfibre fillers, Appl. Clay Sci. 74 (2013) 47–57, https://doi.org/10.1016/j.clay.2012.06.014.
[3] G. Lazzara, G. Cavallaro, A. Panchal, R. Fakhrullin, A. Stavitskaya, V. Vinokurov, Y. Lvov, An assembly of organic-inorganic composites using halloysite clay nanotubes, Curr. Opin. Colloid Interface Sci. 35 (2018) 42–50, https://doi.org/10.1016/j.cocis.2018.01.002.
[4] D.L. Francisco, L.B. Paiva, W. Aldeia, A.B. Lugão, E.A.B. Moura, Noncovalently functionalized halloysite nanotubes for use in reinforced polymer composites, ACS Appl. Nano Mater. 3 (2020) 11510–11516, https://doi.org/10.1021/acsanm.0c02600.
[5] E. Abdullayev, Y. Lvov, Halloysite clay nanotubes as a ceramic "skeleton" for functional biopolymer composites with sustained drug release, J. Mater. Chem. b. 1 (2013) 2894–2903, https://doi.org/10.1039/C3TB20059K.
[6] G. Cavallaro, G. Lazzara, S. Milioto, Nanocomposites based on halloysite nanotubes and sulphated galactan from red seaweed Gloiopeltis: Properties and delivery capacity of sodium diclofenac, Int. J. Biol. Macromol. 234 (2023), 123645, https://doi.org/10.1016/j.ijbiomac.2023.123645.
[7] M.K. Pierchala, M. Makaremi, H.L. Tan, J. Pushpamalar, S. Muniyandy, A. Solouk, S.M. Lee, P. Pasbakhsh, Nanotubes in nanofibers: Antibacterial multilayered polylactic acid/halloysite/gentamicin membranes for bone regeneration application, Appl. Clay Sci. 160 (2018) 95–105, https://doi.org/10.1016/j.clay.2017.12.016.
[8] Y.M. Lvov, M.M. DeVilliers, R.F. Fakhrullin, The application of halloysite tubule nanoclay in drug delivery, Expert Opin. Drug Deliv. 13 (2016) 977–986, https://doi.org/10.1517/17425247.2016.1169271.
[9] Y. Feng, Y. He, X. Lin, M. Xie, M. Liu, Y. Lvov, Assembly of Clay nanotubes on cotton fibers mediated by biopolymer for robust and high-performance hemostatic dressing, Adv. Healthc. Mater. 12 (2023) 2202265, https://doi.org/10.1002/adhm.202202265.
[10] R. Li, Y. Zhang, Z. Lin, Q. Lei, Y. Liu, X. Li, M. Liu, G. Wu, S. Luo, H. Wang, X. Zheng, L. Li, N. Ao, Z. Zha, Injectable halloysite-g-chitosan hydrogels as drug carriers to inhibit breast cancer recurrence, Compos. Part B Eng. 221 (2021), 109031, https://doi.org/10.1016/j.compositesb.2021.109031.
[11] A. Panchal, G. Fakhrullina, R. Fakhrullin, Y. Lvov, Self-assembly of clay nanotubes on hair surface for medical and cosmetic formulations, Nanoscale. 10 (2018) 18205–18216, https://doi.org/10.1039/c8nr05949g.
[12] A. Melnyk, O. Chyhyrynets, G. Lazzara, Encapsulation of α-lipoic acid in halloysite nanotubes, Appl. Sci. 13 (2023) 10214, https://doi.org/10.3390/app131810214.
[13] L. Ghezzi, A. Spepi, M. Agnolucci, C. Cristani, M. Giovannetti, M.R. Tiné, C. Duce, Kinetics of release and antibacterial activity of salicylic acid loaded into halloysite nanotubes, Appl. Clay Sci. 160 (2018) 88–94, https://doi.org/10.1016/j.clay.2017.11.041.
[14] G. Gorrasi, R. Pantani, M. Murariu, P. Dubois, PLA/Halloysite Nanocomposite Films: Water Vapor Barrier Properties and Specific Key Characteristics, Macromol. Mater. Eng. 299 (2014) 104–115, https://doi.org/10.1002/mame.201200424.
[15] G. Gorrasi, V. Senatore, G. Vigliotta, S. Belviso, R. Pucciariello, PET–halloysite nanotubes composites for packaging application: Preparation, characterization and analysis of physical properties, Eur. Polym. J. 61 (2014) 145–156, https://doi.org/10.1016/j.eurpolymj.2014.10.004.
[16] X. Zhao, Y. Luo, P. Tan, M. Liu, C. Zhou, Hydrophobically modified chitin/halloysite nanotubes composite sponges for high efficiency oil-water separation, Int. J. Biol. Macromol. 132 (2019) 406–415, https://doi.org/10.1016/j.ijbiomac.2019.03.219.
[17] N. Danyliuk, J. Tomaszewska, T. Tatarchuk, Halloysite nanotubes and halloysite-based composites for environmental and biomedical applications, J. Mol. Liq. 309 (2020), https://doi.org/10.1016/j.molliq.2020.113077.
[18] J. Kurczewska, M. Cegłowski, G. Schroeder, PAMAM-halloysite Dunino hybrid as an effective adsorbent of ibuprofen and naproxen from aqueous solutions, Appl. Clay Sci. 190 (2020), https://doi.org/10.1016/j.clay.2020.105603.
[19] M.M. Calvino, L. Lisuzzo, G. Cavallaro, G. Lazzara, S. Milioto, Halloysite based geopolymers filled with wax microparticles as sustainable building materials with enhanced thermo-mechanical performances, J. Environ. Chem. Eng. 10 (2022), https://doi.org/10.1016/j.jece.2022.108594.
[20] B. Micó-Vicent, F.M. Martínez-Verdú, A. Novikov, A. Stavitskaya, V. Vinokurov, E. Rozhina, R. Fakhrullin, R. Yendluri, Y. Lvov, Stabilized dye-pigment formulations with platy and tubular nanoclays, Adv. Funct. Mater. 28 (2018) 1703553, https://doi.org/10.1002/adfm.201703553.
[21] O. Owoseni, Y. Su, S. Raghavan, A. Bose, V.T. John, Hydrophobically modified chitosan biopolymer connects halloysite nanotubes at the oil-water interface as complementary pair for stabilizing oil droplets, J. Colloid Interface Sci. 620 (2022) 135–143, https://doi.org/10.1016/j.jcis.2022.03.142.
[22] A. Panchal, L.T. Swientoniewski, M. Omarova, T. Yu, D. Zhang, D.A. Blake, V. John, Y.M. Lvov, Bacterial proliferation on clay nanotube Pickering emulsions for oil spill bioremediation, Colloids Surf. B Biointerfaces. 164 (2018) 27–33, https://doi.org/10.1016/j.colsurfb.2018.01.021.
[23] E. Zandi-Mehri, L. Taghavi, F. Moeinpour, I. Khosravi, S. Ghasemi, Designing of hydroxyl terminated triazine-based dendritic polymer/halloysite nanotube as an efficient nano-adsorbent for the rapid removal of Pb(II) from aqueous media, J. Mol. Liq. 360 (2022), 119407, https://doi.org/10.1016/j.molliq.2022.119407.

[24] J. Zare Pirhaji, F. Moeinpour, A. Mirhoseini Dehabadi, S.A. Yasini Ardakani, Synthesis and characterization of halloysite/graphene quantum dots magnetic nanocomposite as a new adsorbent for Pb(II) removal from water, J. Mol. Liq. 300 (2020), 112345, https://doi.org/10.1016/j.molliq.2019.112345.
[25] A. Kausar, M. Iqbal, A. Javed, K. Aftab, Z.-H. Nazli, H.N. Bhatti, S. Nouren, Dyes adsorption using clay and modified clay: A review, J. Mol. Liq. 256 (2018) 395–407, https://doi.org/10.1016/j.molliq.2018.02.034.
[26] S. Sadjadi, M.M. Heravi, M. Malmir, Pd@HNTs-CDNS-g-C3N4: A novel heterogeneous catalyst for promoting ligand and copper-free Sonogashira and Heck coupling reactions, benefits from halloysite and cyclodextrin chemistry and g-C3N4 contribution to suppress Pd leaching, Carbohydr. Polym. 186 (2018) 25–34, https://doi.org/10.1016/j.carbpol.2018.01.023.
[27] S. Sadjadi, G. Lazzara, M. Malmir, M.M. Heravi, Pd nanoparticles immobilized on the poly-dopamine decorated halloysite nanotubes hybridized with N-doped porous carbon monolayer: A versatile catalyst for promoting Pd catalyzed reactions, J. Catal. 366 (2018) 245–257, https://doi.org/10.1016/j.jcat.2018.08.013.
[28] L. Lisuzzo, G. Cavallaro, S. Milioto, G. Lazzara, Halloysite nanotubes as nanoreactors for heterogeneous micellar catalysis, J. Colloid Interface Sci. 608 (2022) 424–434, https://doi.org/10.1016/j.jcis.2021.09.146.
[29] Y. Liu, H. Guan, J. Zhang, Y. Zhao, J.-H. Yang, B. Zhang, Polydopamine-coated halloysite nanotubes supported AgPd nanoalloy: An efficient catalyst for hydrolysis of ammonia borane, Int. J. Hydrog. Energy. 43 (2018) 2754–2762, https://doi.org/10.1016/j.ijhydene.2017.12.105.
[30] Y. Liu, J. Zhang, H. Guan, Y. Zhao, J.-H. Yang, B. Zhang, Preparation of bimetallic Cu-Co nanocatalysts on poly (diallyldimethylammonium chloride) functionalized halloysite nanotubes for hydrolytic dehydrogenation of ammonia borane, Appl. Surf. Sci. 427 (2018) 106–113, https://doi.org/10.1016/j.apsusc.2017.08.171.
[31] S. Sadjadi, F. Koohestani, G. Pareras, M. Nekoomanesh-Haghighi, N. Bahri-Laleh, A. Poater, Combined experimental and computational study on the role of ionic liquid containing ligand in the catalytic performance of halloysite-based hydrogenation catalyst, J. Mol. Liq. 331 (2021), 115740, https://doi.org/10.1016/j.molliq.2021.115740.
[32] S. Sadjadi, N. Abedian-Dehaghani, M.M. Heravi, X. Zhong, P. Yuan, J. Duran, A. Poater, N. Bahri-Laleh, Clay-supported acidic ionic liquid as an efficient catalyst for conversion of carbohydrates to 5-hydroxymethylfurfural, J. Mol. Liq. 382 (2023), 121847, https://doi.org/10.1016/j.molliq.2023.121847.
[33] L. Zhang, X. Xu, S. Jiang, L. Wei, K. Xi, Y. Lei, X. Cheng, J. Yin, Y. Gao, Halloysite nanotubes modified poly(vinylidenefluoride-co-hexafluoropropylene)-based polymer-in-salt electrolyte to achieve high-performance Li metal batteries, J. Colloid Interface Sci. 645 (2023) 45–54, https://doi.org/10.1016/j.jcis.2023.04.127.
[34] W. Wang, Y. Yang, H. Luo, J. Zhang, Design of advanced separators for high performance Li-S batteries using natural minerals with 1D to 3D microstructures, J. Colloid Interface Sci. 614 (2022) 593–602, https://doi.org/10.1016/j.jcis.2022.01.148.
[35] F. Liu, L. Bai, H. Zhang, H. Song, L. Hu, Y. Wu, X. Ba, Smart H2O2-Responsive Drug Delivery System Made by Halloysite Nanotubes and Carbohydrate Polymers, ACS Appl. Mater. Interfaces. 9 (2017) 31626–31633, https://doi.org/10.1021/acsami.7b10867.
[36] B. Tang, H. Zhang, C. Cheng, H. Jiang, L. Bai, X. Ba, Y. Wu, Development of halloysite nanotube-based hydrogel with colorimetric H2O2-responsive character, Appl. Clay Sci. 212 (2021), 106230, https://doi.org/10.1016/j.clay.2021.106230.
[37] L. Lisuzzo, G. Cavallaro, P. Pasbakhsh, S. Milioto, G. Lazzara, Why does vacuum drive to the loading of halloysite nanotubes? The key role of water confinement, J. Colloid Interface Sci. 547 (2019) 361–369, https://doi.org/10.1016/j.jcis.2019.04.012.
[38] C. Duce, V.D. Porta, E. Bramanti, B. Campanella, A. Spepi, M.R. Tiné, Loading of halloysite nanotubes with BSA, α -Lac and β -Lg: a Fourier transform infrared spectroscopic and thermogravimetric study, Nanotechnology 28 (2017), 055706.
[39] L. Lisuzzo, G. Cavallaro, S. Milioto, G. Lazzara, Coating of silk sutures by Halloysite/wax Pickering emulsions for controlled delivery of eosin, Appl. Clay Sci. 247 (2024), 107217, https://doi.org/10.1016/j.clay.2023.107217.
[40] M. Makaremi, P. Pasbakhsh, G. Cavallaro, G. Lazzara, Y.K. Aw, S.M. Lee, S. Milioto, Effect of morphology and size of halloysite nanotubes on functional pectin bionanocomposites for food packaging applications, ACS Appl. Mater. Interfaces. 9 (2017) 17476–17488, https://doi.org/10.1021/acsami.7b04297.
[41] Z. Luo, H. Song, X. Feng, M. Run, H. Cui, L. Wu, J. Gao, Z. Wang, Liquid Crystalline Phase Behavior and Sol-Gel Transition in Aqueous Halloysite Nanotube Dispersions, Langmuir. 29 (2013) 12358–12366, https://doi.org/10.1021/la402836d.
[42] J. Cao, X. Kang, B. Bate, Microscopic and physicochemical studies of polymer-modified kaolinite suspensions, Colloids Surf. Physicochem. Eng. Asp. 554 (2018) 16–26, https://doi.org/10.1016/j.colsurfa.2018.06.019.
[43] M.M. Calvino, G. Cavallaro, L. Lisuzzo, S. Milioto, G. Lazzara, Separation of halloysite/kaolinite mixtures in water controlled by sucrose addition: The influence of the attractive forces on the sedimentation behavior, Colloids Surf. Physicochem. Eng. Asp. 641 (2022), 128530, https://doi.org/10.1016/j.colsurfa.2022.128530.
[44] G. Cavallaro, G. Lazzara, V. Taormina, D. Cascio, Sedimentation of halloysite nanotubes from different deposits in aqueous media at variable ionic strengths, Colloids Surf. Physicochem. Eng. Asp. 576 (2019) 22–28, https://doi.org/10.1016/j.colsurfa.2019.05.038.
[45] H. Wu, J. Xie, M. Lattuada, J. Kohlbrecher, M. Morbidelli, Effect of primary particle size and salt concentration on the structure of colloidal gels, J. Phys. Chem. c. 115 (2011) 931–936, https://doi.org/10.1021/jp103100k.
[46] J. Russo, J. Fiegel, N.K. Brogden, Effect of Salt Form on Gelation and Drug Delivery Properties of Diclofenac-Loaded Poloxamer Gels for Delivery to Impaired Skin, Pharm. Res. 39 (2022) 2515–2527, https://doi.org/10.1007/s11095-022-03356-1.
[47] A. Fernández-Nieves, A. Fernández-Barbero, F.J. De las Nieves, Salt effects over the swelling of ionized mesoscopic gels, J. Chem. Phys. 115 (2001) 7644–7649, https://doi.org/10.1063/1.1403002.
[48] Y. Tu, X. Zhang, L. Wang, Effect of salt treatment on the stabilization of Pickering emulsions prepared with rice bran protein, Food Res. Int. 166 (2023), https://doi.org/10.1016/j.foodres.2023.112537.
[49] J. Li, W. Zhang, T. Tang, L. Gu, Y. Su, Y. Yang, C. Chang, Q. Han, Thermal gelation and digestion properties of hen egg white: Study on the effect of neutral and alkaline salts addition, Food Chem. 409 (2023), 135263, https://doi.org/10.1016/j.foodchem.2022.135263.
[50] G.J. Churchman, P. Pasbakhsh, D.J. Lowe, B.K.G. Theng, Unique but diverse: some observations on the formation, structure and morphology of halloysite, Clay Miner. 51 (2016) 395–416, https://doi.org/10.1180/claymin.2016.051.3.14.
[51] A. Pramanik, A. Sciortino, M. Reale, P. Pasbakhsh, G. Cavallaro, M. Cannas, G. Lazzara, F. Messina, Naturally occurring halloysite nanotubes as light scatterers for stable random lasing applications, ACS Appl. Nano Mater. 6 (2023) 15896–15905, https://doi.org/10.1021/acsanm.3c02840.
[52] Mark Raven, Peter Self, Dehydration and intercalation behavior of the unique "Patch Clay" halloysite using in-situ XRD, in: EUROCLAY -, Int. Conf. Clay Sci. Technol. (2019).
[53] T. Le Ba, A.Q. Alkurdi, I.E. Lukács, J. Molnár, S. Wongwises, G. Gróf, I.M. Szilágyi, A novel experimental study on the rheological properties and thermal conductivity of halloysite nanofluids, Nanomaterials 10 (2020) 1834, https://doi.org/10.3390/nano10091834.
[54] M. Anvari, M. Tabarsa, R. Cao, S. You, H.S. Joyner Melito, S. Behnam, M. Rezaei, Compositional characterization and rheological properties of an anionic gum from Alyssum homolocarpum seeds, Food Hydrocoll. 52 (2016) 766–773, https://doi.org/10.1016/j.foodhyd.2015.07.030.
[55] L.S. Tavares, L.A. Junqueira, Í.C. de Oliveira Guimarães, J.V. de Resende, Cold extraction method of chia seed mucilage (*Salvia hispanica* L.): effect on yield and rheological behavior, J. Food Sci. Technol. 55 (2018) 457–466, https://doi.org/10.1007/s13197-017-2954-4.
[56] J.L. Dávila, M.A. d'Ávila, Laponite as a rheology modifier of alginate solutions: Physical gelation and aging evolution, Carbohydr. Polym. 157 (2017) 1–8, https://doi.org/10.1016/j.carbpol.2016.09.057.
[57] P.G. Lawrence, Y. Lapitsky, Ionically cross-linked poly(allylamine) as a stimulus-responsive underwater adhesive: Ionic strength and pH effects, Langmuir. 31 (2015) 1564–1574, https://doi.org/10.1021/la504611x.
[58] G.E. Cunningham, F. Alberini, M.J.H. Simmons, J.J. O'Sullivan, Understanding the effects of processing conditions on the formation of lamellar gel networks using a rheological approach, Chem. Eng. Sci. 242 (2021), https://doi.org/10.1016/j.ces.2021.116752.
[59] T. Domenech, S.S. Velankar, On the rheology of pendular gels and morphological developments in paste-like ternary systems based on capillary attraction, Soft Matter. 11 (2015) 1500–1516, https://doi.org/10.1039/c4sm02053g.
[60] G.A. Valencia, I.C.F. Moraes, L.H.G. Hilliou, R.V. Lourenço, P.J.D.A. Sobral, Nanocomposite-forming solutions based on cassava starch and laponite: Viscoelastic and rheological characterization, J. Food Eng. 166 (2015) 174–181, https://doi.org/10.1016/j.jfoodeng.2015.06.006.
[61] E.A. Appel, M.W. Tibbitt, M.J. Webber, B.A. Mattix, O. Veiseh, R. Langer, Self-assembled hydrogels utilizing polymer-nanoparticle interactions, Nat. Commun. 6 (2015), https://doi.org/10.1038/ncomms7295.
[62] Y. Zhang, W. Gao, Y. Chen, T. Escajadillo, J. Ungerleider, R.H. Fang, K. Christman, V. Nizet, L. Zhang, Self-assembled colloidal gel using cell membrane-coated nanosponges as building blocks, ACS Nano. 11 (2017) 11923–11930, https://doi.org/10.1021/acsnano.7b06968.
[63] E.O. Castrejón-González, V.E. Márquez Baños, J.F. Javier Alvarado, V. Rico-Ramírez, J. Castillo-Tejas, H. Jiménez-Islas, Rheological model for micelles in solution from molecular dynamics, J. Mol. Liq. 198 (2014) 84–93, https://doi.org/10.1016/j.molliq.2014.07.016.
[64] Y.-R. Wang, Q. Yang, Y.-J. Li-Sha, H.-Q. Chen, Structural, gelation properties and microstructure of rice glutelin/sugar beet pectin composite gels: Effects of ionic strengths, Food Chem. 346 (2021), https://doi.org/10.1016/j.foodchem.2020.128956.
[65] A.D. Drozdov, J.D. Christiansen, The effects of pH and ionic strength on the volume phase transition temperature of thermo-responsive anionic copolymer gels, Polymer. 221 (2021), https://doi.org/10.1016/j.polymer.2021.123637.
[66] S. Shafiei-Sabet, W.Y. Hamad, S.G. Hatzikiriakos, Ionic strength effects on the microstructure and shear rheology of cellulose nanocrystal suspensions, Cellulose. 21 (2014) 3347–3359, https://doi.org/10.1007/s10570-014-0407-z.